JOURNAL OF GEOPHYSICAL RESEARCH, VOL. 115, B07106, doi:10.1029/2009JB006943, 2010

Seismic structure of an oceanic core complex at the Mid-Atlantic Ridge, 22°19′N

Anke Dannowski,[1] Ingo Grevemeyer,[1] Cesar R. Ranero,[2] Georges Ceuleneer,[3] Marcia Maia,[4] Jason Phipps Morgan,[5] and Pascal Gente[4]

Received 1 September 2009; revised 8 January 2010; accepted 25 January 2010; published 24 July 2010.

[1] We present results from a seismic refraction and wide-angle experiment surveying an oceanic core complex on the Mid-Atlantic Ridge at 22°19′N. Oceanic core complexes are settings where petrological sampling found exposed lower crustal and upper mantle rocks, exhumed by asymmetric crustal accretion involving detachment faulting at magmatically starved ridge sections. Tomographic inversion of our seismic data yielded lateral variations of *P* wave velocity within the upper 3 to 4 km of the lithosphere across the median valley. A joint modeling procedure of seismic *P* wave travel times and marine gravity field data was used to constrain crustal thickness variations and the structure of the uppermost mantle. A gradual increase of seismic velocities from the median valley to the east is connected to aging of the oceanic crust, while a rapid change of seismic velocities at the western ridge flank indicates profound differences in lithology between conjugated ridge flanks, caused by un-roofing lower crust rocks. Under the core complex crust is approximately 40% thinner than in the median valley and under the conjugated eastern flank. Clear *PmP* reflections turning under the western ridge flank suggest the creation of a Moho boundary and hence continuous magmatic accretion during core complex formation.

Citation: Dannowski, A., I. Grevemeyer, C. R. Ranero, G. Ceuleneer, M. Maia, J. P. Morgan, and P. Gente (2010), Seismic structure of an oceanic core complex at the Mid-Atlantic Ridge, 22°19′N, *J. Geophys. Res.*, *115*, B07106, doi:10.1029/2009JB006943.

1. Introduction

[2] Lithospheric accretion along the slow-spreading Mid-Atlantic Ridge (MAR) is driven by two contrasting modes: (1) asymmetric accretion involving active detachment faulting and core complex formation and (2) symmetric magmatic accretion with abyssal hill formation on both conjugated ridge flanks [*Escartin et al.*, 2008]. Oceanic core complexes (OCCs) are lower crustal or upper mantle rocks exhumed at the seafloor by long-lived detachment faults. At some settings they may accommodate extension for 1–2 m.y. [*Tucholke and Lin*, 1994; *Tucholke et al.*, 1998]. Characteristic features of OCCs are blocky topography with dome-shaped structures and often spreading-parallel corrugated surfaces [*Cann et al.*, 1997; *Blackman et al.*, 1998; *Tucholke et al.*, 1998]. Active detachment faulting is associated with near constant levels of seismic activity in a colder thermal regime compared to magmatic segments [*Smith et al.*, 2006; *Escartin et al.*, 2008] and occurs generally at ridge crest discontinuities. However, within the last 5 years OCCs have been recognized to occur nearly randomly along some spreading segments [*Smith et al.*, 2006, 2008].

[3] Spatial and temporal variation in magmatic and tectonic processes leads to a high structural variability at OCCs [*Tucholke and Lin*, 1994; *Cann et al.*, 1997; *Escartin et al.*, 2003; *Smith et al.*, 2006], resulting in different models explaining the observations. *Tucholke et al.* [1998] suggest that core complexes form by a detachment fault rooting at the base of the lithosphere. The onset of amagmatic extension results in detachment faulting and the formation of a detachment that accretes lithospheric mantle and exposes the deep lithosphere. In an alternative model *Dick et al.* [2000] proposed a detachment fault rooting at or near a melt-rich zone near the spreading axis. Continuous magmatic accretion occurs during detachment faulting, exposing mainly gabbros that are deformed at high temperatures and in the presence of melt. A third conceptual model [*Escartin et al.*, 2003] localizes the detachment fault rooting in the shallow lithosphere. During extension active gabbro intrusions and dyke injections occur episodically across the fault zone. They will be exposed during continued extension. The alteration front may correspond to a rheological boundary.

[1]Leibniz Institute of Marine Science at University of Kiel (IFM-GEOMAR), Kiel, Germany.
[2]ICREA at Institut de Ciencias del Mar, CSIC, Barcelona, Spain.
[3]Toulouse University, Observatoire Midi-Pyrénées, Toulouse, France.
[4]Université Européenne de Bretagne, Brest, France.
[5]EAS Department, Cornell University, Ithaca, New York, USA.

0148-0227/10/2009JB006943

[4] These models would predict very different crustal and upper mantle structure at the OCC and the hanging wall preserved in the median valley and at the conjugated ridge flank. The main difference between the models would be the geometry of the crust/mantle boundary (i.e., seismic Moho). While in the amagmatic extension model [*Tucholke et al.*, 1998], the Moho would reach the seafloor under the core complex; the Moho would occur several kilometers below the seafloor in the melt-assisted extension model [*Dick et al.*, 2000]. For the episodically magmatic extension with an alteration front [*Escartin et al.*, 2003], a seismic velocity gradient would be expected rather than a sharp contrast in velocity.

[5] A number of seismic surveys studied OCCs at active spreading ridges like the Atlantis Bank at the Southwest Indian Ridge (SWIR) [*Muller et al.*, 2000; *Dick et al.*, 2000], the Atlantis Massif at the MAR near 30°N [*Canales et al.*, 2004] (MAR), the TAG area at the MAR near 26°N, the Mid-Atlantic Ridge at Kane (MARK) area at the MAR near 23°20′N [*Canales and Collins*, 2000; *Canales and Collins et al.*, 2008; *de Martin et al.*, 2007], and at the MAR 5°S [*Planert et al.*, 2010]. However, they concentrate on the OCC itself and resolve only the upper 1–2 km. Here we will use seismic data to study the crustal and upper mantle structure surveying the seismic velocity structure of an OCC and its associated hanging wall on the conjugated rift shoulder, crossing the Mid-Atlantic Ridge at 22°19′N. A joint modeling approach using both seismic and gravimetric data resolves both the crustal and upper mantle structure.

2. Tectonic Setting

[6] At the Mid-Atlantic Ridge to the south of the Kane transform fault boundary the North American and African plates separate at a rate of 2.5 cm/yr [*Gente et al.*, 1995]. The MARK area to the south of the Kane transform fault has been targeted by a number of seismic refraction studies, yielding a complex and heterogeneous lithospheric architecture dominated by amagmatic extension at the OCC to the south of the Kane transform fault [*Canales et al.*, 2008; *Dick et al.*, 2008; *Toomey et al.*, 1988] and a magmatically dominated mode of lithospheric accretion away from the transform fault [*Purdy and Detrick*, 1986; *Canales and Collins*, 2000]. Further south an area of high seismic activity characterizes the Mid-Atlantic Ridge between 22° 10′N and 22°40′N [*Escartin et al.*, 2008]. This area is situated north of the highly magmatic southward propagating TAMMAR segment. Centered roughly at 22°17′N, a short ridge segment [*Gente et al.*, 1995] that existed for roughly 5 m.y. occurs. Segment boundaries to the north and south, however, are not well defined. The segment length can best be defined by an anomalously deep seafloor, which is roughly 500–1000 m deeper that the seafloor to the north and south. A dome-shaped structure on the western ridge flank at 22°19′N is interpreted as core complex [*Cannat et al.*, 1995] caused by detachment faulting with spreading-parallel corrugations (Figure 1). The core complex is located approximately 10 km off-axis to the west,and its summit occurs at the magnetic anomaly 2, indicating an age of about 1.8 m.y. [*Gente et al.*, 1995].

[7] Figure 1b shows the 22°19′N core complex. Its eastern flank dips at an angle of 42°. The fault intersects the valley surface roughly 6–7 km away from the ridge axis. The next fault block to the east is suggested to be the active fault bounding the axial valley. The break-away is difficult to define using the existing bathymetric data. However, the western end of the dome occurs 20–25 km off the ridge axis and may suggest that the fault system is active for about 2 m.y. Several ridge-parallel features crosscut the core complex and may represent rotated fault (rafted) blocks covering the surface of the detachment fault or secondary ridge parallel fault zones. Further west abyssal hills are aligned to the core complex, though westward a domal structure, possibly a fossil core complex occurs.

3. Geology of the Core Complex

[8] The geological structure of the Mid-Atlantic Ridge at 22°19′N could be derived from two dredge campaigns [*Karson et al.*, 1987; *Cannat et al.*, 1995] and previously unpublished data from a dive of the French submersible *Nautile*. Figure 2 presents results of these studies.

[9] During the TAMMAR cruise with R/V *Nadir* in 1996, the submersible *Nautile* explored during its dive 21 the southeastern slope of the 22°19′N dome along a SE-NW trending ~4 km long transect (Figure 2). Within the median valley the seabed is heavily sedimented. Scattered and isolated angular blocks of serpentinite fallen down from the nearby cliffs occurred rarely. Close to the foothill, a narrow ~E-W trending ridge of mylonitic and amphibolitized gabbros emerged from the sediments. At a depth of 2960 m serpentinized peridotites crop out. Serpentinites are intensely fractured. Further up slope, at 2230 m, a brecciated zone is detected. The breccia is made of fragments of serpentinized peridotites and of metadiabase embedded in a fine matrix made of serpentine, chlorite, and likely clay minerals. The thickness of the brecciated zone reaches several hundred meters and its general orientation is N-S with a subvertical dip. This “cold” contact separates the serpentinites from the overlying outcrops of diabase dykes and basalts. The orientation of the dykes is N-S with a high westward dip (i.e., parallel to the one of the diaclases cutting the serpentinites). At a depth of 2050 m a subhorizontal E-W trending shear zone crosscuts the diabase dykes that are pervasively transformed into an assemblage of chlorite and other green schist facies minerals. The sampled gabbros and serpentinites are described in detail in the Appendix. *Ghose et al.* [1996] gave petrological data on the ultramafic rocks dredged south of this core complex at the 22°10′N discontinuity that terminates the segment end toward the south.

[10] In contrast to the ultramafic and gabbroic rocks that have been sampled on the western high, sampling of the eastern conjugated ridge flank and in the median valley suggest that the lithology is dominated by basalts and diabases [*Karson et al.*, 1987; *Cannat et al.*, 1995], supporting a mode of asymmetric lithospheric accretion. Thus, core complex formation unroofed the footwall of lower crustal and upper mantle rocks on the western flank and transferred the hanging wall of upper crust to the east. Seafloor topography supports this interpretation. Blocky topography characterizes the western ridge flank, while the eastern

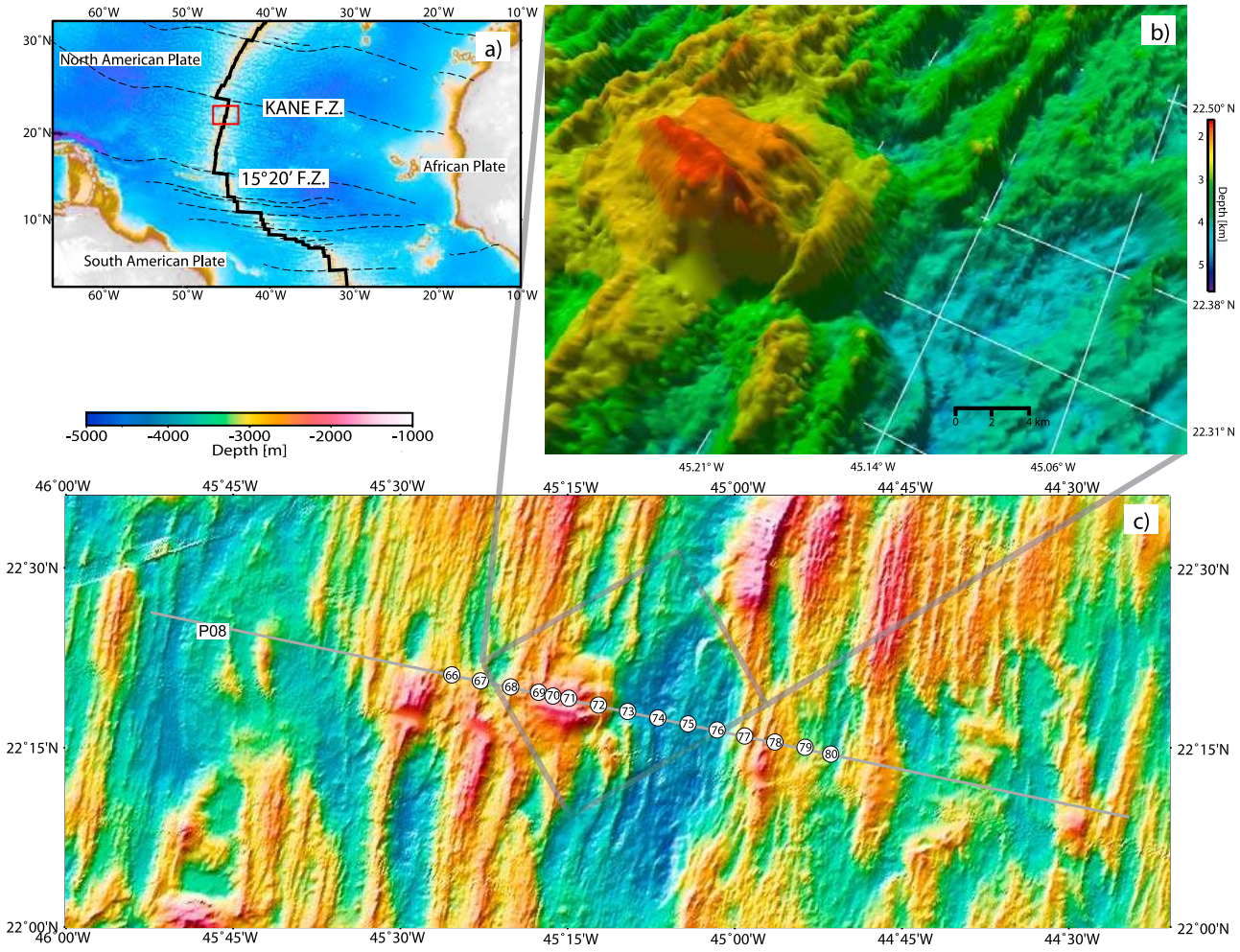

Figure 1. Bathymetric maps of the study area. (a) Overview of the global tectonic features. The red rectangle marks the survey field south of MARK area. (b) Domed structure in a 3-D view. This is the key feature of the study and is interpreted as an oceanic core complex. (c) Overview of the seismic line with its deployed instruments (15 Ocean Bottom Hydrophones).

conjugated flank shows linear abyssal hills and small basins (Figure 1c).

4. Seismic Experiment and Gravity Data

[11] START HERE In December of 2003 and January of 2004 the COSTMAR cruise (M60/2) was conducted aboard the German research vessel *Meteor* at the Mid-Atlantic Ridge between 21°30′N and 22°30′N. Profile p08 crossed the 22°19′N core complex. Fifteen ocean bottom hydrophones [*Flueh and Bialas*, 1996] were deployed along the 150 km long seismic transect, sampling the structure of a portion of the Mid-Atlantic Ridge. Two 32 L Bolt air guns, operating at a pressure of 130 bar, were used as seismic sources. Guns were fired at a shot interval of 60 s, resulting at a ship's speed of about 4 knots over ground into a shot spacing of approximately 120 m. Ocean bottom hydrophones (OBHs) were deployed by free fall, using Global Positioning System (GPS) for drop point positioning. The instrument locations were further constraints using water wave arrival times from air gun shots collected while the ship was navigated with GPS. Before deploying the OBHs, all clocks were rated against a GPS DCF77 time signal. After recovery, the OBH internal clock was rated against GPS time to determine the drift, in order to calculate time corrections. Timing errors were generally less than 30 ms and were assumed to be related to a linear drift over the time of deployment. Data passed an antialiasing filter and were continuously recorded with a sampling rate of 100 or 125 Hz on all OBHs. The data were played back and split into single shot records stored as receiver gathers in SEG-Y format. Spectral analysis and filter tests show that the seismic energy is in a band ranging from 4 to 20 Hz. We ran this test for both near-offset and far-offset traces and chose a time- and offset-dependent filtering approach. In addition, a predictive deconvolution was applied and previously amplitudes were multiplied by distance to partly compensate the spherical divergence, simultaneously showing the level of both seismic signal and ambient noise. Data examples can be found in Figure 3.

[12] Gravity data used in our study were obtained in 1991 during the SEADMA1 cruise with the French research

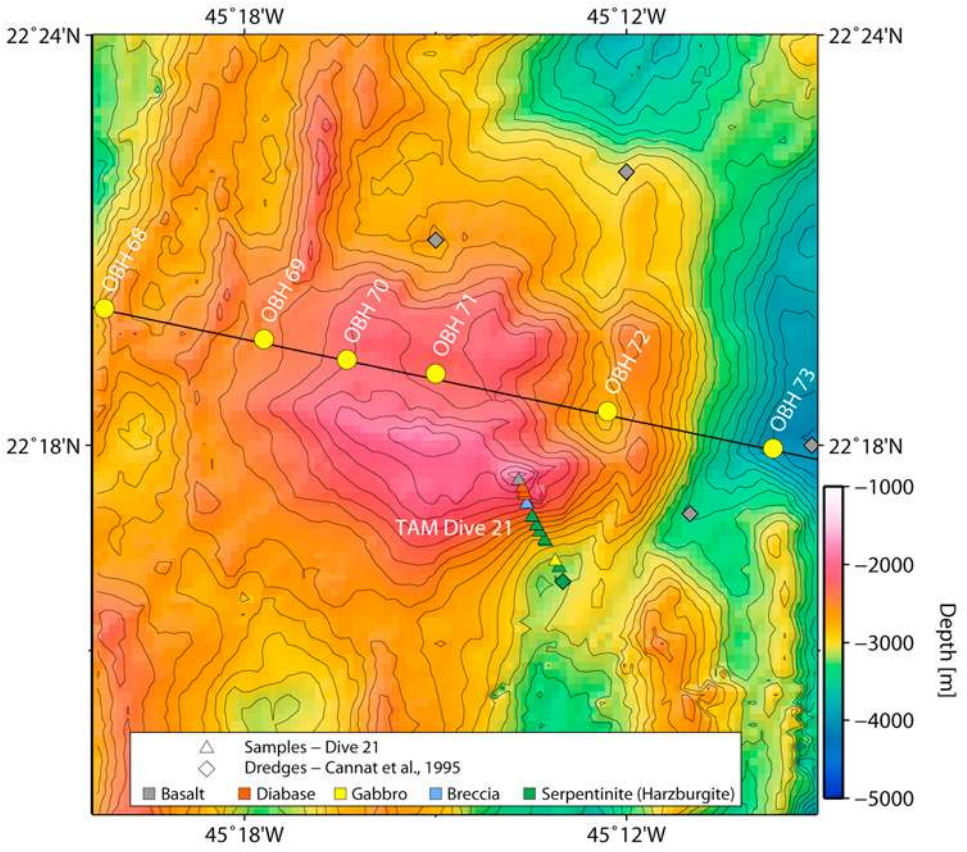

Figure 2. Bathymetric map of the core complex showing the location of the Tammar-Dive21 and the seismic line including stations that cover the massif. Dredges from studies of the MARK area are included.

vessel *l'Atalante* [*Gente et al.*, 1991, 1995] with a KSS30 Bodenseewerk gravity meter [*Maia and Gente*, 1998].

5. Modeling Procedure

[13] Seismic data recorded along the profile have generally been of excellent quality. However, it is interesting to note that seismic wide-angle reflection data have just been recorded on a few stations, though refracted arrivals of energy turning in the uppermost mantle have been imaged to offsets of 60–80 km. Thus, record sections generally lack high-quality wide-angle reflection phases from the crust/mantle boundary (*PmP*), perhaps related to a weak trace-to-trace correlation of seismic phases due to scattering and diffractions caused by the rough seafloor relief. However, lateral changes in the lithology at Moho depth may also govern the occurrence of reflected arrivals. The fact that only a few record sections provided clear *PmP* reflections as secondary arrivals in a credible manner had governed the inversion and modeling procedure. Thus, seismic travel time tomography without wide-angle constraints on the geometry of the seismic Moho may suffer from a trade-off between changes in seismic velocity and layer geometry. Therefore, due to the complexity of the area, different modeling techniques like seismic tomographic inversion, ray trace modeling, and gravity modeling were used to resolve the crustal and upper mantle structure. We used seismic travel time tomography of crustal phases (*Pg*) to yield the seismic structure of the crust. In a second step, however, we included Moho reflections; constraining crustal thickness were *PmP* phases that have been sampled. Constraints on the crustal thickness along the entire profile were further obtained using forward modeling of upper mantle turning rays (*Pn*) and gravity data. The seismic and gravimeric Moho were derived using an iterative approach, updating crustal thickness simultaneously for both data sets. In addition, the modeling procedure yielded upper mantle seismic velocities and densities.

5.1. Results From Tomographic Inversion

[14] Seismic data at small offsets of up to 30 km have a high signal-to-noise ratio (Figure 3), allowing a clear identification of a crustal refraction branch (*Pg*). The 2305 hand-picked travel times (picking error < 40 ms) show a strong scattering at equal shot-receiver distances. This strong variation in the travel curves is perhaps related to both the rough seafloor topography and a strong variation in the shallow seismic structure along the profile, as reported elsewhere for OCCs [*Canales et al.*, 2008].

[15] We used the tomographic method of *Korenaga et al.* [2000] to invert *P* wave travel times, yielding a seismic velocity model for the uppermost 3–5 km of the crust. A regular grid with uniform horizontal grid cells of 200 m and a vertical increasing spacing from 50 to 170 m was used.

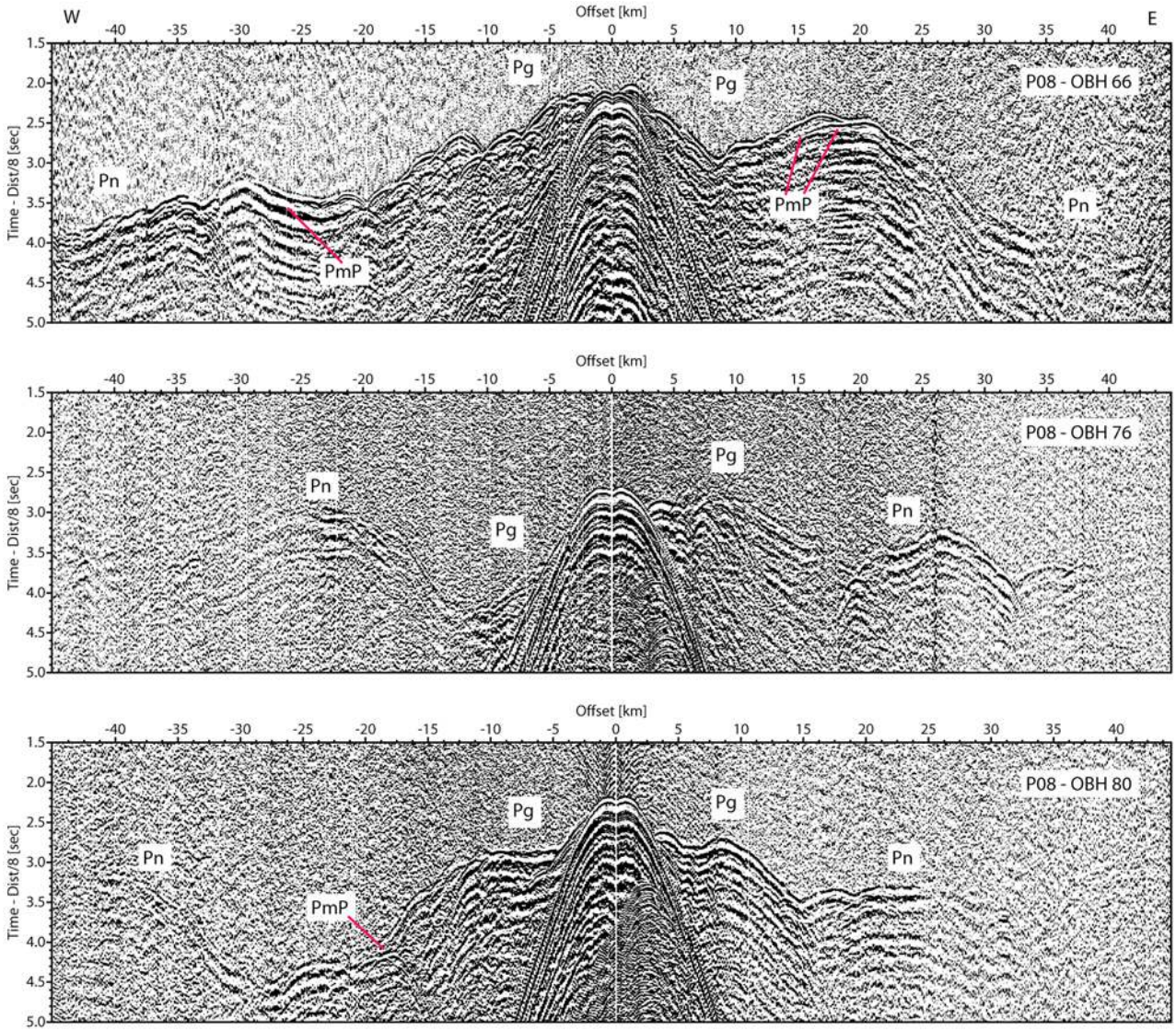

Figure 3. Seismic sections of reduced velocity to 8 km/s are shown as data examples of the seismic line P08. The signal-to-noise ratio is high up to an offset of 40 km, and the refracted waves of the crust and the mantle are highly visible at most of the stations and up to 80 km for some OBHs. However, the mantle reflection phase cannot be continuously identified over all stations. Interpreted seismic arrivals have been labeled: *Pg* (turning rays within the crust), *Pn* (turning rays in the upper mantle), and *PmP* (reflected rays at the Moho).

The grid hangs below the seafloor and was parameterized at a spacing of 500–600 m. During inversion we used layer stripping, inverting first for the upper crustal arrivals or near offset picks, and proceeded with the larger offset picks, leading to a robust model of the refracted data for the crust. A standard 1-D starting velocity model had been defined as reference model for 2-D tomographic inversion. The 1-D model was derived using constraints from previous seismic refraction surveys at the MAR to the south of Kane transform boundary [*Purdy and Detrick*, 1986; *Canales et al.*, 2000]. However, different starting models were tested to yield the robustness of inversion result. Tests included several half-space models with different velocity gradients and several layered models. The final solution, however, depended only weakly on the starting model.

[16] A strong lateral variation in crustal structure is well displayed in the seismic velocity model (Figure 4). The eastern flank of the ridge shows typical features for normal oceanic crust with a high velocity gradient in layer 2 and a relative constant thickness of 1.5–2.2 km. The estimated velocity rises from 3.2 km/s at the top of igneous crust to about 6.5 km/s at 2 km below the seafloor. The lower crust has a lower gradient, and velocities increase slowly to 7.0–7.2 km/s near the expected bottom of crust. In the median valley, seismic velocities are slowest; low velocities of 2.3–2.4 km/s were observed in the first few hundred meters below the seafloor in the eastern part of the axial valley. Velocity reaches 6.5 km/s at the depth of 4 km below the seafloor with a low velocity gradient in the lower crust. Further west, approaching the dome-shaped core complex,

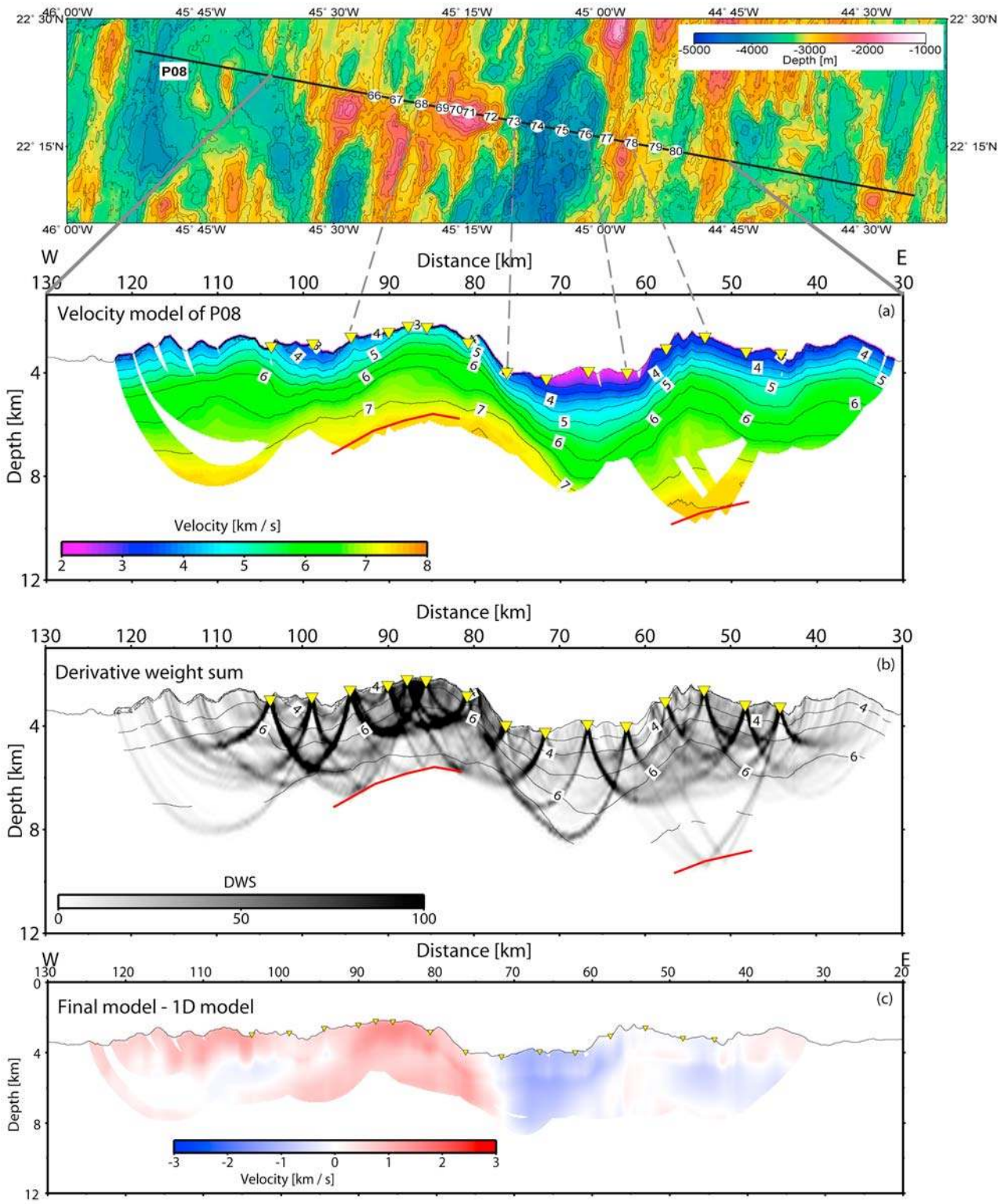

Figure 4. (a) Preferred final *P* wave velocity model of the upper crust after five iterations. The interval of the contour lines is 0.5 km/s. Crustal picks up to an offset of 20 km and wide-angle reflection arrivals have been used for the inversion tomography. The upper part of this figure, the bathymetric map, shows where stations and profile are situated. (b) Resolution of the model, the ray coverage of the tomographic inversion. (c) Velocity perturbations from average oceanic crust at the MAR.

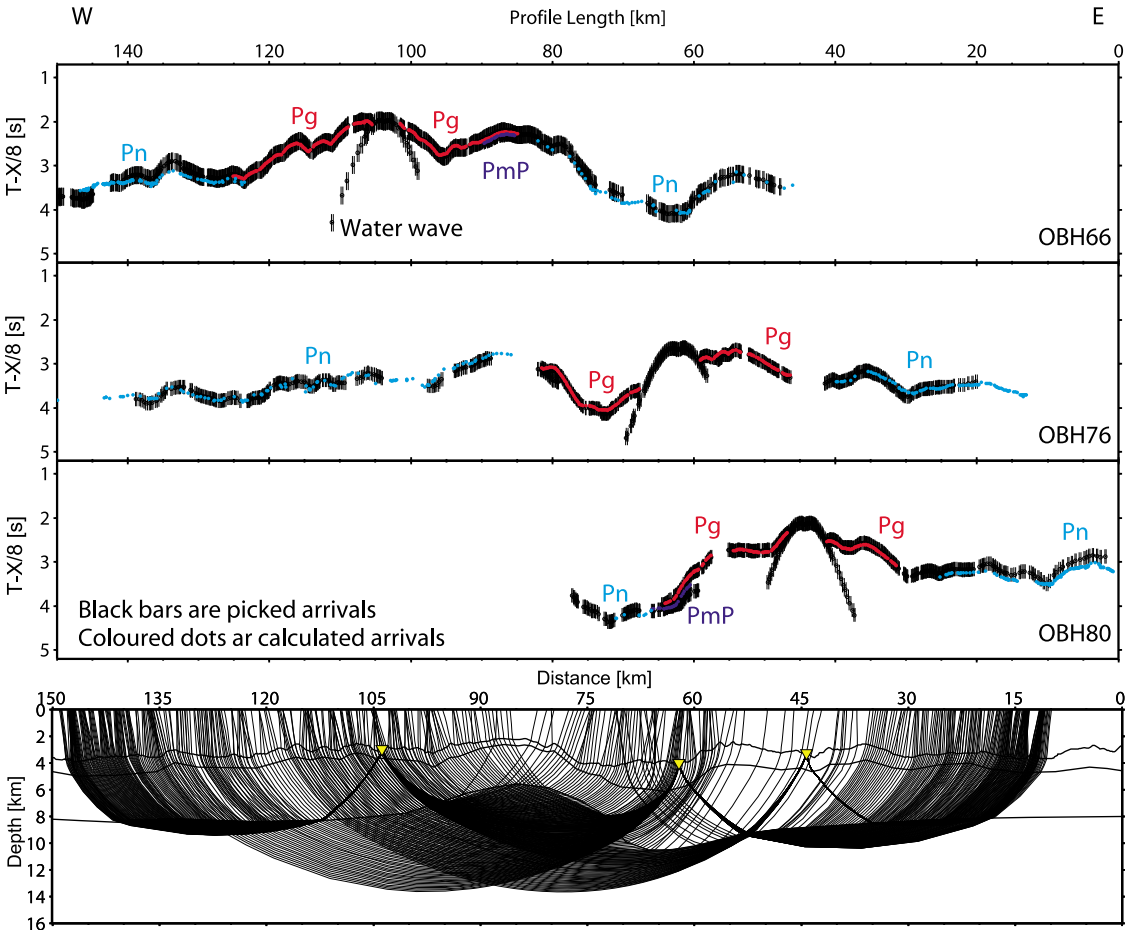

Figure 5. Travel time fits for the three data examples in Figure 3. Observed (vertical bars) and predicted (colored dots) travel times for the final velocity model: *Pg* (red) and *PmP* (dark blue) from the inversion (red) and Pn from the forward modeling (light blue). Pn arrivals are constraining the upper mantle structure beneath the massif. At larger offsets, rays do penetrate, but the data quality is too low to gain trustable picks.

velocities increase to values of 3–4 km/s at the seabed, and the uppermost crust is characterized by a steep vertical velocity gradient. Lower crustal velocities of more than 7 km/s were imaged at already 1.5 km below the seafloor. To the west of the core complex, crust is more similar to the eastern flank, with a high velocity gradient in layer 2 and moderately increasing velocity in the lower crust, layer 3, reaching velocities of 7.1–7.2 km/s at a depth of 4 km below seafloor.

[17] Crustal thickness could be derived at to two patches along the profile, where a number of Moho wide-angle reflections were observed. Generally, wide-angle phases had good quality where the seafloor was smooth. Fortunately, OBH80 on the eastern flank provided a clear *PmP* phase, indicating a crustal thickness of 6 km for the eastern flank. In addition, OBH66 to OBH71 on top of the core complex provided *PmP* phases. Here, crustal thickness is ~3.5 km, indicating approximately 40% thinner crust.

[18] In Figures 5 and 6 the observed and calculated travel times are compared. The final RMS misfit is 49 ms and the $\chi^2 \sim 2.01$ for the crustal phases. The inversions converged from an initial $\chi^2 = 13.08$ after five iterations. The ray coverage (Figure 4b) constrains the model.

5.2. Combined Seismic and Gravity Modeling

[19] A benefit of using a ray tracing forward method was the application of a joint modeling approach using observed travel times, including mantle arrivals (*Pn*), and the marine free-air gravity field. We used MacRay [*Luetgert*, 1992] to generate a model satisfying both gravity and seismic data, where *Pn* arrivals and gravity data provide useful constraints on the crustal thickness and structure of the uppermost mantle.

[20] Seismic velocities have been converted to density model using different empirical relationships for upper and lower crust: $\rho = 3.81–6/v_p$ [*Carlson and Herrick*, 1990] for the upper crust; $\rho = 0.375 + 0.375*v_p$ [*Birch*, 1961] for gabbroic crust found in the lower crust. The mantle was initially assumed to have a constant density of 3.3 g/cm^3. For upper crust seismic velocities less than 4 km/s a value of 2.4 g/cm^3 has been assumed, using constraints from an ocean bottom gravity study at the Juan de Fuca Ridge

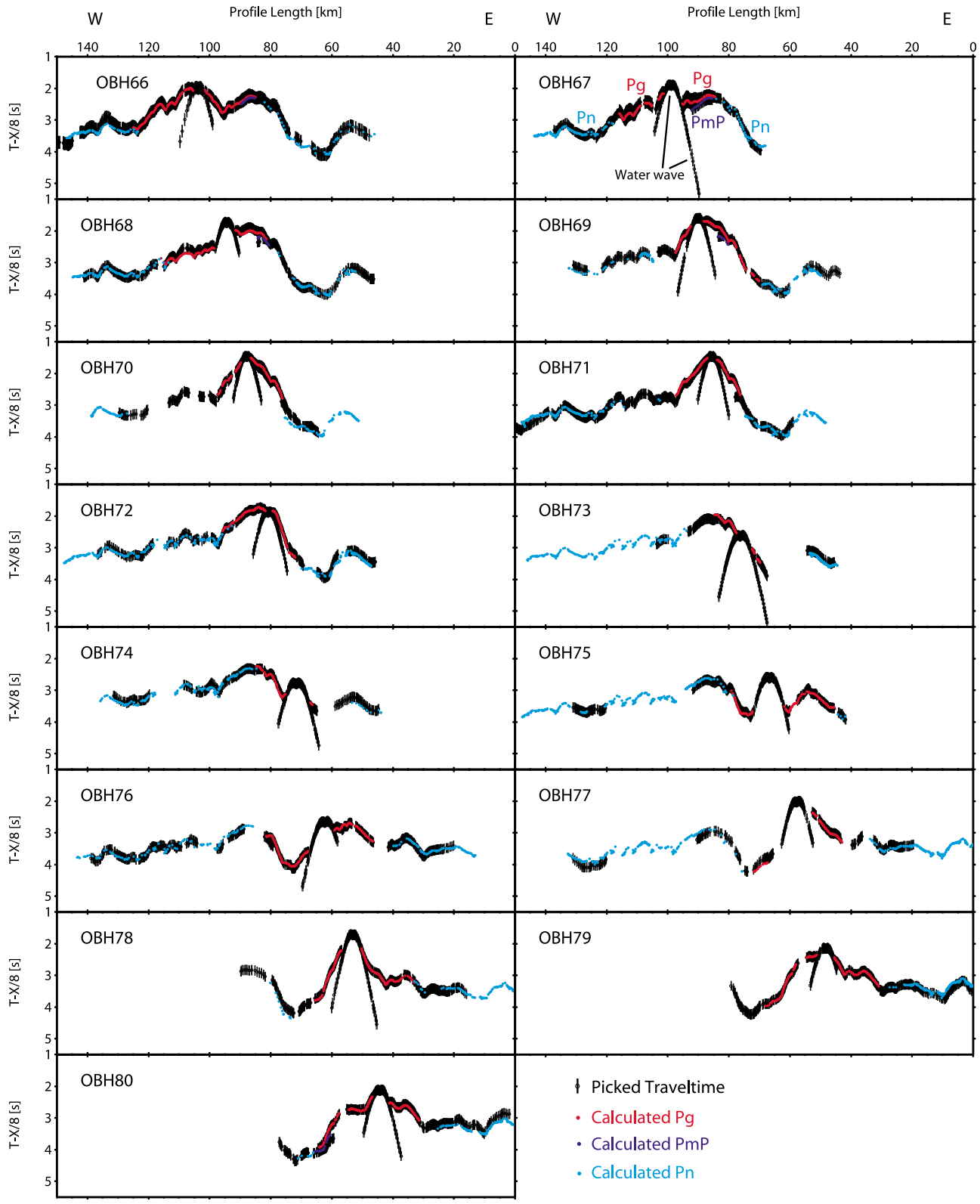

Figure 6. Travel time fits for all stations along profile 8. Observed (vertical bars) and predicted (colored dots) travel times for the final velocity model: *Pg* (red) and *PmP* (dark blue) from the inversion (red) and *Pn* from the forward modeling (light blue). *Pn* arrivals are constraining the upper mantle structure beneath the massif. At larger offsets, rays do penetrate, but the data quality is too low to gain trustable picks.

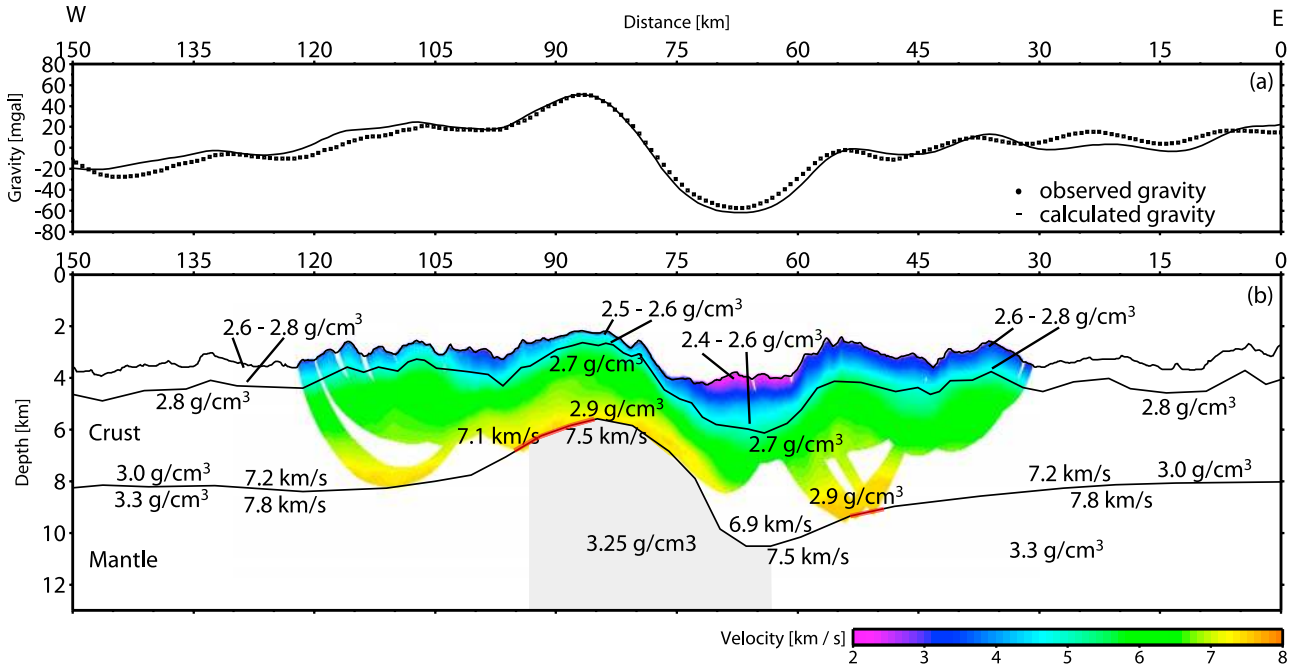

Figure 7. Combined seismic and gravity forward modeling: (a) gravity fit and (b) preferred final seismic velocity and density model. The colored section is the result of the joint near-offset first arrival and wide-angle reflection tomographic inversion. The deeper structures as well as the density values result from forward modeling using the raytracing method [*Luetgert*, 1992]. The gray shaded area in the mantle shows the area with lowered densities. The red thickened lines of the crust–mantle boundary indicate the parts where the Moho is constraint by seismic wide-angle reflection arrivals.

[*Stevenson et al.*, 1994]. Figure 7 shows that there is not only a strong lateral variation in the density and velocity field at crustal levels but also density variations in the mantle. As a result of 934 picks of *Pn* arrivals distributed along the entire profile, we could image both the geometry of the seismic Moho and the velocity structure of the uppermost mantle. The modeling strategy was to start with a flat Moho. However, profound changes had to be introduced to fit both *Pn* arrivals and gravity field data. Away from the ridge crest, velocities of 7.8 km/s fit the *Pn* branches best. Below the median valley and the western ridge flank velocities decrease to 7.5 km/s.

[21] Potential field methods are nonunique, and the interpretation of seismic results may suffer from the trade-off between seismic velocity and the thickness of a layer. Nevertheless, density contrast both at the water/seabed interface and the Moho caused strong lateral variations of about 100 mGal in the observed gravity field. The topographic effect alone could not explain the observed anomaly over the massif, supporting a shallower mantle (higher density material) underlying the core complex. The final model (Figure 7) shows reduced velocities and density in the mantle below the median valley and the core complex and reduced crustal thickness under the detachment fault, indicating crustal thinning caused by faulting. The RMS residual for the gravity modeling is 5.22 mGal. The observed and calculated travel times are plotted and compared in Figures 5 and 6.

[22] A few clear *PmP* branches have been observed and were used to constrain the final model derived from ray tracing and gravity modeling. It is interesting to note that a few *PmP* branches sampled both the normal roughly 6 km thick crust away from the core complex and the portion of thinner crust under the core complex, supporting crustal thickness variations from the forward modeling. In addition, the occurrence of *PmP* arrivals suggests that a well-defined Moho discontinuity has been developed, indicating ongoing magmatic accretion during detachment faulting and hence supporting the model of *Dick et al.* [2000].

6. Discussion

6.1. Upper Crustal Structure

[23] The seismic data reported here is a rare data set covering both conjugated ridge flanks and hence the footwall and hanging wall of a detachment fault. We obtained a strong variation in seismic velocities within the upper 3–4 km across the ridge axis. Velocities near the seabed vary by more than ±1.1 km/s. A distinct feature is a very rapid increase in *P* wave velocity where the median valley approaches the western ridge flank. Velocities increase from about 2.3 to 4.5 km/s over a distance of 5–7 km and are fastest below the dome-shaped core complex. On the conjugated eastern ridge flank, however, seismic velocities increase more gradually (Figure 4).

[24] Seismic velocities may increase while crust ages. This phenomenon is related to hydrothermal precipitation of secondary alteration products into open pore spaces and cracks, decreasing the porosity and hence increasing seismic velocities [e.g., *Grevemeyer and Weigel*, 1996; *Carlson*,

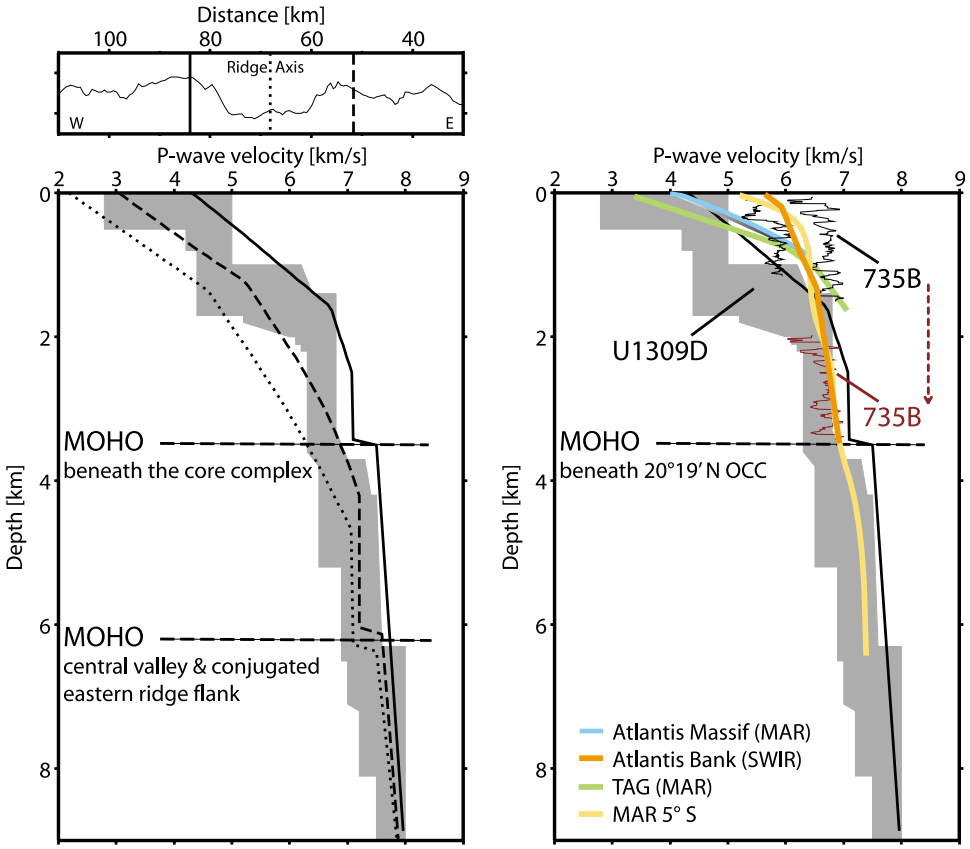

Figure 8. Velocity versus depth profiles. (left) Representation of the ridge axis (dashed line), the core complex to the west (solid), and the opposite side at same offset (dotted). The gray zone denotes the range of typical velocity profiles for 0–7 Ma oceanic crust after *White et al.* [1992]. This diagram supports the interpretation of a change in lithology. (right) Comparison to other studied OCC's including sonic logs of the IODP hole U1309D and ODP hole 735B (IODP Lamont logging database), seismic models of the TAG area [*de Martin et al.*, 2007], Atlantis Massif [*Canales et al.*, 2008], Atlantis Bank [*Muller et al.*, 2000], and MAR 5°S [*Planert et al.*, 2010]. The sonic log data have been plotted twice; the brown plot has been moved downward to better compare the gabbroic section of our model with the gabbroic velocities from the drilling.

1998; *Grevemeyer et al.*, 1999]. The impact of hydrothermal activity on the seismic structure causes a gradual change in seismic velocities [*Grevemeyer et al.*, 1999; *Nedimović et al.*, 2008]. A rapid change as observed at the OCC, however, may support a change in lithology. Sampling supports this interpretation. Dredges from the median valley floor and the eastern ridge shoulder provided basaltic seafloor, while sampling provided a wide range of rock types, including serpentinites and gabbroic rocks from the core complex (Figure 2).

[25] Different models of core complex formation suggest fundamental differences in lithology. Thus, while melt-assisted extension supports that the internal structure of the OCC is dominantly grabboic [*Dick et al.*, 2000], amagmatic extension may unroof mantle rocks [*Tucholke et al.*, 1998]. Petrologic interpretation of seismic velocities might be non-unique. For mantle rocks, for example, seismic *P* wave velocity decreases with increasing degree of serpentinization. Velocities of >8 km/s characterize unaltered peridiotites, whereas 100% serpentinized peridotite shows decreased velocities of 4.5 km/s [*Carlson and Miller*, 2003]. Thus, serpentinization may turn velocities of mantle peridiotites into velocities typical for lower crustal or upper crustal rocks. Fracturing may even further decrease seismic velocities. Gabbroic rocks generally have velocities of 6.7–7.1 km/s. Like for serpentinites, fracturing may also decrease values significantly. Thus, based on seismic velocity data alone, it is difficult to discriminate between different rock types. Nevertheless, *Canales et al.* [2008] found a correlation between seismic velocities and lithology. They found that areas where serpentinites have been dredged were characterized by *P* wave velocities of <3.5 km/s, whereas velocities of >4 km/s generally occur where gabbros have been found. Our data at the 22°19′N core complex support fast velocities close to the seabed (3–4 km/s), reaching ~7 km/s at 1.5 km below the seafloor (Figures 4 and 8). In the context of the interpretation by *Canales et al.* [2008], our seismic data suggest that lower crustal rocks have been brought to shallow depth; thus, the core complex is suggested to be dominantly composed of gabbroic rocks (Figure 9). A

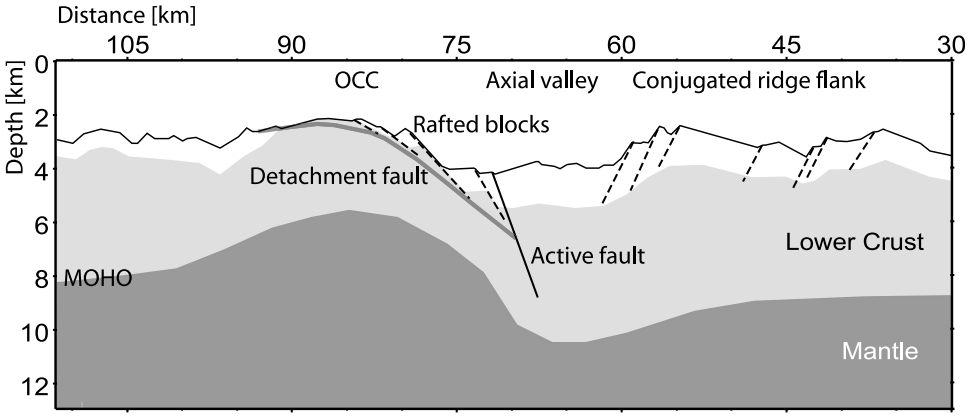

Figure 9. The geological interpretation of the seismic modeling. After initiation of the detachment the crust becomes approximately 40% thinner compared to normal oceanic crust. The mantle wells up while the detachment fault grows. To the east normal faulting occurs. The plate boundary moves from the center westward to the active fault of the core complex. The model is plotted with 2.5× vertical exaggeration.

rather low seismic velocity gradient below the upper 1.5 km supports these observations. An alteration front separating hydrated from dry mantle, as for example predicted by *Escartin et al.* [2003], would rather cause a steep gradient instead of a first-order discontinuity. Thus, the observation of wide-angle reflections (our *PmP* arrivals) favors our interpretation of a lithological boundary separating crustal from mantle rocks.

6.2. Crustal and Upper Mantle Structure

[26] Recent drilling campaigns at OCCs [*Blackman et al.*, 2006; *Escartin et al.*, 2003; *Ildefonse et al.*, 2007] obtained mostly gabbroic rocks and hence support our interpretation. For example, IODP hole U1309D penetrated roughly to a depth of >1.4 km and sampled dominantly gabbroic rocks of a highly primitive nature at the central dome of the Atlantis Massif to the north of the Atlantis transform fault boundary of the Mid-Atlantic Ridge. The velocity–depth relation found by *Canales et al.* [2008] and the sonic log data from U1309D show strong similarities to our results for the depth interval of 1–1.5 km. Velocities and the velocity gradient are slightly higher, though (Figure 8).

[27] However, sampling on the southern wall of the 22°19′N core complex sampled mainly serpentinized peridotites at the lower footwall (dive21), suggesting either that the core complex is laterally heterogeneous or that the surface lithology did not represent the internal structure of OCCs. Similar features have been found elsewhere. For example, dredges from a rifted inside corner high at the MAR near 5°S found that serpentinites have been smeared as fault gouges along the corrugated slip surface but that the core complex internally was largely plutonic [*Reston et al.*, 2002, *Planert et al.*, 2010]. However, a micro-earthquake survey in that region [*Tilmann et al.*, 2004] showed that a sharp transition exists between the magmatic segment center and the amagmatic segment end. This transition may reflect a change in rheology and lithology. Thus, it may suggest that near ridge crest discontinuities some of the melt extracted from the asthenosphere crystallizes in the mantle and hence part of the crust is made of fractured and serpentinized ultramafics [*Cannat et al.*, 1995; *Cannat*, 1996], dominating the lithology at segment ends.

[28] Drilling into the Atlantis Bank at the Southwest Indian Ridge, ODP hole 735B, also provided mainly gabbroic rocks from the core complex [*Dick et al.*, 2000]. *Dick et al.* [2000] proposed a detachment fault rooting at or near a melt-rich zone near the ridge axis, where a continuous magmatic crust is formed during detachment faulting, which exposes mainly gabbros. In such a scenario a Moho boundary is formed and therefore constrains our interpretation that lower crustal material forms the oceanic core complex, while upper mantle has not been exposed. In other scenarios of core complex formation, where extension occurs during amagmatic extension [*Tucholcke et al.*, 1998] or where the detachment fault is rooted in the shallow lithosphere [*Escartin et al.*, 2003], we would not expect the formation of a profound density or velocity contrast at Moho depth. Thus, hydrothermal circulation in exposed, and a fractured mantle may cause an alteration front [*Escartin et al.*, 2003; *Python et al.*, 2007]. However, alteration would cause a gradual change in velocity and density instead of a sharp contrast, as derived from the joint forward modeling of mantle refractions and gravity field data. Furthermore, the occurrence of *PmP* reflections supports a significant velocity contrast at depth. The presence of gabbros, intensely sheared in high-temperature conditions (amphibolite facies), sampled with *Nautile* on the steep southeastern wall of the dome (see discussion in section 3), is typical for magmatic processes. Additionally, the sampled basalts (Figure 2) on top of the core complex, in the median valley, and on the conjugated ridge flank indicate that magmatism took place while the detachment fault was exposed. These features support the interpretation that the active fault was rooted in a zone of magmatic accretion. The sonic log data of hole 735 show high velocities typical for gabbro. These data and the velocity–depth profile of the seismic velocity model from *Muller et al.* [2000] have been plotted in Figure 8. In contrast to our OCC (dredged basalts and diabase), at the Atlantis Bank predominantly gabbroic rocks have been sampled. Thus, for comparison, the log data have been

shifted downward below 1.5 km to compare the lithological similar sections between both core complexes. For the deeper part (deeper than 1.5 km), the velocity structure is very similar to our final velocity model, and the velocities are slightly slower.

[29] *PmP* reflections, observed in our seismic data (Figures 3 and 4), and the density contrast obtained in our modeling support crust that is roughly ~40% thinner under the core complex (Figure 7), suggesting that accretion of the American plate is dominated by faulting rather than magmatic construction during the past ~2 million years. In contrast, crust under the median valley and eastern ridge flank, representing the hanging wall of the fault system, is roughly 5 km thick, and seafloor topography shows generally ridge parallel abyssal hill fabric. It is therefore reasonable to classify these areas as oceanic crust accreted dominantly by magmatic processes.

[30] Reduced seismic velocities in the upper mantle might be caused to some extent by high mantle temperatures and the existence of a few percent of melt. *Grevemeyer et al.* [1998], for example, detected at the East Pacific Rise that mantle velocities increase from <7.5 km/s near the ridge crest to >8 km/s in rough 10 m.y. old crust. At slow-spreading ridges, faults penetrating down to mantle depth [*Huang and Solomon*, 1988] may provide paths for seawater to reach the upper mantle. Evidence from ophiolites supports the penetration of high-temperature hydrothermal fluids down to mantle depths [*Leblanc et al.*, 1991; *Benoit et al.*, 1999; *Python et al.*, 2007]. Hydration and hence serpentinization may therefore affect seismic velocities. However, as mantle velocities seem to increase from ~7.5 km/s at the ridge crest to 7.8 km/s roughly 60 km off-axis, we favor the interpretation that changes in the thermal regime dominate this evolutionary process.

6.3. Core Complex Formation

[31] The critical question is whether the proposed detachment fault causing the core complex is still active or inactive. Unfortunately, no fault plane solutions are available for this area. However, existing fault plain solutions for different areas at mid-ocean ridges support that faulting generally occurs at normal faults dipping at 40°–60° [*Huang and Solomon*, 1987, 1988]. The distribution of earthquakes from hydroacoustic monitoring indicate that near 22°19′N seismicity is concentrated below the axial valley [*Smith et al.*, 2003], while the core complex itself is almost aseismic. A similar feature has been observed in the TAG area at 26°10′N using a local network of ocean bottom seismic stations [*de Martin et al.*, 2007]. In addition to the distribution of seismicity within the area, the deployment provided earthquake hypocenters, indicating an active steep fault (~70°) that is rooted in the median valley. Seismic velocities derived from crustal phases provided a velocity structure similar to our tomographic inversion, suggesting that lower crustal rocks are being exhumed in a detachment fault, which appears to roll over to a shallow dip of 20° and become aseismic at a depth of ~3 km. This scenario is further supported by seismic data from fossil oceanic detachment faults [*Ranero and Reston*, 1999].

[32] In contrast to the TAG detachment fault, bathymetric data from the 22°19′N core complex suggest that the inactive portion of the detachment fault surface is covered by rafted blocks (Figure 1c). Rafted blocks on top of the OCCs have been described between 13° and 15°N [*Smith et al.*, 2008] and in the Canary Basin, Central Atlantic [*Reston et al.*, 2004]. The occurrence of rafted blocks is supported by diabase dykes and basalts sampled from the top, the northern and the eastern slopes of the massif (Figure 2). Along with our final seismic velocity and density model the observed features could generally be explained by a "rolling-hinge" model proposed by *Buck* [1988]. The model assumes that faults have ranges of optimal orientations to the principal stresses. According to the Mohr-Coulomb criterion, shear failure will occur once the shear strength and internal friction of a rock body are overcome. Rock mechanics experiments and numerical simulations show that when a fault is rotated away from the optimum angle for shear, frictional sliding along a fault may become more difficult than creating a new fault through unfractured rock [e.g., *Nur et al.*, 1986; *Buck*, 1988]. In this scenario, a normal fault, when significantly rotated from the optimum angle of slip, relative to the crustal stress field, is replaced by a new planar fault orientated in the optimum direction. Thus, the low angle detachment fault remains inactive and is covered with rafted blocks. The geometry of the detachment fault and uplift of the dome-shaped core complex is further affected by the low flexural rigidity of zero-aged crust.

[33] Core complex formation at the Atlantis Bank at the Southwest Indian Ridge caused a strong asymmetry in both lithospheric structure and spreading rate. *Baines et al.* [2008] reported that 80% of plate motion was accommodated by the detachment fault, causing a northward migration of the ridge crest with respect to adjacent segments spreading symmetrically. Therefore, *Baines et al.* [2008] hypothesized that asymmetric spreading rates may be a characteristic feature of other detachment faults. Unfortunately, magnetic data from the 22°19′N core complex are not as detailed as from the Atlantis Bank. However, the existing data from *Gente et al.* [1995] suggest that lithospheric accretion at the MAR near 22°19′N occurs symmetrical with respect to the spreading rate of the African and North American plates.

[34] Based on our seismic velocity model, bathymetry and seafloor ages from magnetic data [*Gente et al.*, 1995], we derived an evolutionary model for the core complex formation at 22°19′N (Figure 9). Roughly 1.9 m.y. ago magma supply decreases and core complex formation initiated. In our scenario, the initial fault dips at ~60° and is located in the median valley. When rotated away from its optimum dip, slip stops, and a new fault is created. Tectonic extension causes crustal thinning of 40% and exposed gabbroic lower crust of about 20 km. Crustal thinning, flexural fault rotation, and perhaps serpentinization cause an uplift of the core complex, resulting into the prominent dome-shaped massif of the 22°19′N core complex.

7. Conclusions

[35] Across the Mid-Atlantic Ridge at 22°19′N seismic refraction data show large lateral variations of the upper crustal *P* wave velocity structure. We observe the lowest velocities in the median valley, increasing gradually toward the east and rapidly near the western ridge flank. The western flank shows a prominent high of an oceanic core complex. Velocities up to 4.5 km/s may indicate exposure of

highly fractured lower crustal rocks. Roughly 1.5 km below the seabed, seismic velocities reach 7 km/s. Fast material under the dome-shaped core complex clearly support gabbroic rocks occurring at shallow depth, suggesting that the rapid change in seismic velocities is related to a lithological change caused by the unroofing of the crust. In contrast, seismic velocity data suggest that the lithosphere at the conjugated eastern flank was accreted by processes dominated by magmatic construction and hence show a typical velocity depth distribution expected for normal oceanic crust.

[36] Joint raytracing and gravity modeling suggest that crust under the core complex is approximately 2 km thinner than under the conjugated ridge flank. The velocity and density contrast as well as a few clear *PmP* reflections support that a Moho boundary was created during core complex formation, suggesting that the detachment fault is rooted in a zone of magmatic accretion at 2–4 km depth.

[37] We favor the interpretation that the core complex was formed by a mechanism similar to the rolling-hinge model by *Buck* [1988]. The core complex formation started roughly 1.9 m.y. ago and is perhaps still active. Even though accretion seems to be highly asymmetric in terms of the lithospheric structure of conjugated ridge flanks, accretion of North American and African plates occur at similar rates. A major discontinuity could explain the sharp transition between the crustal lithology beneath the massif and ultramafics occurring at the southern wall [*Karson et al.*, 2006]. However, this transition might be controlled by the thermal structure, favoring melt being trapped in the mantle during melt extraction at cool segment ends [e.g., *Cannat et al.*, 1995; *Cannat*, 1996].

Appendix

[38] The mylonitic gabbro sampled at the base of the section contains small porphyroclasts of clinopyroxene (cpx) and of plagioclase (plg) up to 0.5 mm in size; they are embedded in a fine-grained matrix made of a mosaic of plg and amphibole a few tens of microns in size with sutured grain boundaries. Plg porphyroclasts present well-developed mechanical twins. Cpx porphyroclasts have generally rounded shapes and are heavily recrystallized and transformed into hornblende on their border. The protolith of this mylonite was a gabbro devoid of olivine and of oxides. The porphyroclasts allow us to infer the primary igneous phase composition. Plg porphyroclasts have an average An content of 0.55. Some porphyroclasts present a slight inverse zoning with An ranging from 0.48 to 0.57, but most of them are quite homogeneous in composition. Cpx porphyroclasts are augites with a Mg# of 0.78, a low Cr_2O_3 content (0.1 wt%), a moderate Al_2O_3 content (2.5 wt%), and a high TiO_2 content (0.7 wt%). These values are typical of evolved cumulates from normal mid-oceanic ridge basalt (NMORB) [e.g., *Elthon*, 1987; *Natland and Dick*, 1996]. With respect to gabbros drilled in the nearby ODP Site 923, the samples follow the differentiation trend, indicating that they derive from similar parent melts. The composition of these gabbros is the one expected for cumulates from mid-oceanic ridge basalt (MORB) of the MARK area [*Ross and Elthon*, 1997].

[39] Amphibole from the matrix is a common green hornblende (average formula is $Na_{0.5}Ca_{1.8}(Mg,Fe)_{4.7}(OH,CL,F)_{2.0}Si_{7.0}Al_{1.0}$). Plagioclase in the matrix has the same An content as the one of porphyroclasts. These data indicate that deformation occurred in conditions of high temperature (typically around 500°C–600°C) and of water saturation. No evidence for overprint by a lower $T°$ deformation episode is found in this sample (no retromorphic mineral assemblages, nor catactlastic deformation). The amphibolized gabbro can be interpreted as a witness of a ductile, possibly detachment fault, rooted in a former magma body that accommodated shearing at high temperature.

[40] Although 100% serpentinized (which prevented any geochemical analysis of the primary minerals), the serpentinized peridotites have preserved a coarse-grained (up to 1 cm) mosaic textures diagnostic of hot working in low stress and high temperature (~1200°C) conditions. Such textures are classically attributed to deformation related to "asthenospheric" mantle flow [*Ceuleneer et al.*, 1988]. The orientation of the deformation plane, measured on one sample reoriented on board is subhorizontal, a situation similar to the one observed in the nearby peridotite massif drilled at DSDP Site 920 [*Ceuleneer and Cannat*, 1997]. No overprint of lower temperature deformation (500°C–600°C), equivalent to the one recorded by the foothill amphibolized gabbro, has been observed on this outcrop. The rock is harzburgitic in composition (i.e., a prealteration assemblage of olivine and orthopyroxene). Interstitial grains (likely former clinopyroxene) diagnostic of precipitation from a melt are observed in a few samples.

[41] **Acknowledgments.** We are grateful for the support of captain Kull and his crew of RV *Meteor* for their excellent support during the expedition M60/2. The manuscript benefited from the review of two anonymous referees. The research was funded by the German Science Foundation (DFG) (grants Mo 961-5/1 Ra 925-5/1 Gr 1964-8/2+8/3).

References

Baines, A. G., M. J. Cheadle, B. E. John, and J. J. Schwartz (2008), The rate of oceanic detachment faulting at Atlantis Bank, SW Indian Ridge, *Earth Planet. Sci. Lett.*, *273*, 105–114, doi:10.1016/j.epsl.2008.06.013.

Benoit, M., G. Ceuleneer, and M. Polvé (1999), The remelting of hydrothermally altered peridotite at mid-ocean ridges by intruding mantle diapir, *Nature*, *402*, 514–518, doi:10.1038/990073.

Birch, F. (1961), The velocity of compressional waves in rocks to 10 kilobars, part 2, *J. Geophys. Res.*, *66*(B7), 2199–2224, doi:10.1029/JZ066i007p02199.

Blackman, D. K., J. R. Cann, B. Janssen, and D. K. Smith, (1998), Origin of extensional core complexes: Evidence from the Mid-Atlantic Ridge at Atlantis fracture zone, *J. Geophys. Res.*, *103*(B9), 21,315–21,333.

Blackman, D. K., B. Ildefonse, B. E. John, Y. Ohara, D. J. Miller, and C. J. MacLeod (2006), *Proc. Integrated Ocean Drilling Program*, *vols. 304/305*, The Geological Society of America, College Station, Texas.

Buck, W. R. (1988), Flexural rotation of normal faults, *Tectonics*, *7*(5), 959–973, doi:10.1029/TC007i005p00959.

Canales, J. P., and J. A. Collins, (2000), Seismic structure across the rift valley of the Mid-Atlantic Ridge at 23°20′ (MARK area): Implications for crustal accretion processes at slow spreading ridges, *J. Geophys. Res.*, *105*(B12), 28,411–28,425.

Canales, J. P., B. E. Tucholke, and J. A. Collins (2004), Seismic reflection imaging of an oceanic detachment fault: Atlantis megamullion (Mid-Atlantic Ridge, 30°10′N), *Earth Planet. Sci. Lett.*, *222*, 543–560, doi:10.1016/j.epsl.2004.02.023.

Canales, J. P., B. E. Tucholke, M. Xu, J. A. Collins, and D. L. DuBois (2008), Seismic evidence for large-scale compositional heterogeneity of oceanic core complexes, *Geochem. Geophys. Geosyst.*, *9*, Q08002, doi:10.1029/2008GC002009.

Cann, J. R., D. K. Blackman, D. K. Smith, E. McAllister, B. Janssen, S. Mello, E. Avgerinos, A. R. Pascoe, and J. Escartin (1997), Corrugated slip surfaces formed at ridge-transform intersections on the Mid-Atlantic Ridge, *Nature*, *385*, 329–332, doi:10.1038/385329a0.

Cannat, M. (1996), How thick is the magmatic crust at slow spreading ridges? *J. Geophys. Res.*, *101*(B2), 2847–2857, doi:10.1029/95JB03116.

Cannat, M., et al. (1995), Thin crust, ultramafic exposures, and rugged faulting patterns at the Mid-Atlantic Ridge (22°–24°N), *Geology*, *23*, 49–52, doi:10.1130/0091-7613(1995)023<0049:TCUEAR>2.3.CO;2.

Carlson, R. L. (1998), Seismic velocities in the uppermost oceanic crust: Age dependence and the fate of layer 2A, *J. Geophys. Res.*, *103*(B4), 7069–7077, doi:10.1029/97JB03577.

Carlson, R. L., and C. N. Herrick (1990), Densities and porosities in the oceanic crust and their variations with depth and age, *J. Geophys. Res.*, *95*(B6), 9153–9170, doi:10.1029/JB095iB06p09153.

Carlson, R. L., and D. J. Miller (2003), Mantle wedge water contents estimated from seismic velocities in partially serpentinised peridotites, *Geophys. Res. Lett.*, *30*(5), 1250, doi:10.1029/2002GL016600.

Ceuleneer, G., and M. Cannat (1997), High temperature ductile deformation of the site 920 peridotites, in Proc. Ocean Drilling Program, Scientific Results, vol. 153, edited by J. A. Karson, M. Cannat, D. J. Miller, and D. Elthon, pp. 23–34, Ocean Drilling Program, College Station, Tex., doi:10.2973/odp.proc.sr.153.002.1997.

Ceuleneer, G., A. Nicolas, and F. Boudier (1988), Mantle flow patterns at an oceanic spreading centre: The Oman peridotites record, *Tectonophysics*, *151*, 1–26, doi:10.1016/0040-1951(88)90238-7.

de Martin, B. J., R. A. Sohn, J. P. Canales, and S. E. Humphris (2007), Kinematics and geometry of active detachment faulting beneath the Trans-Atlantic Geotraverse (TAG) hydrothermal field on the Mid-Atlantic Ridge, *Geology*, *35*, 711–714, doi:10.1130/G23718A.1.

Dick, H. J. B., et al. (2000), A long in situ section of the lower ocean crust: Results of ODP Leg 176 drilling at the Southwest Indian Ridge, *Earth Planet. Sci. Lett.*, *179*, 31–51, doi:10.1016/S0012-821X(00)00102-3.

Dick, H. J. B., M. A. Tivey, and B. E. Tucholke (2008), Plutonic foundation of a slow-spreading ridge segment: Oceanic core complex at Kane Megamullion, 23°30′N, 45°20′W, *Geochem. Geophys. Geosyst.*, *9*, Q05014, doi:10.1029/2007GC001645.

Elthon, D. (1987), Petrology of gabbroic rocks from the Mid-Cayman Rise spreading center, *J. Geophys. Res.*, *92*(B1), 658–682, doi:10.1029/JB092iB01p00658.

Escartin, J., C. Mével, C. J. MacLeod, and A. M. McCaig (2003), Constraints on deformation conditions and the origin of oceanic detachments: The Mid-Atlantic Ridge core complex at 15°45′N, *Geochem. Geophys. Geosyst.*, *4*(8), 1067, doi:10.1029/2002GC000472.

Escartin, J., D. K. Smith, J. Cann, H. Shouten, C. L. Langmuir, and S. Escrig (2008), Central role of detachment faults in accretion of slow spreading oceanic lithosphere, *Nature*, *455*, 790–794, doi:10.1038/nature07333.

Flueh, E. R., and J. Bialas (1996), A digital, high data capacity ocean bottom recorder for seismic investigations, *Int. Underwater Syst. Design*, *18*, 18–20.

Gente, P., et al. (1991), Geometry of past and present-day segmentation of the Mid-Atlantic Ridge south of Kane fracture zone, *Eos Trans, AGU*, *72*(17), Spring Meet. Suppl., 477.

Gente, P., R. A. Pockalny, C. Durand, C. Deplus, M. Maia, G. Ceuleneer, C. Mével, M. Cannat, and C. Laverne (1995), Characteristics and evolution of the segmentation of the Mid-Atlantic Ridge between 20°N and 24°N during the last 10 million years, *Earth Planet. Sci. Lett.*, *129*, 55–71, doi:10.1016/0012-821X(94)00233-O.

Ghose, I., M. Cannat, and M. Seyler (1996), Transform fault effect on mantle melting in the MARK area (Mid-Atlantic Ridge south of the Kane transform), *Geology*, *24*, 1139–1142, doi:10.1130/0091-7613(1996)024<1139:TFEOMM>2.3.CO;2.

Grevemeyer, I., and W. Weigel (1996), Seismic velocities of the uppermost igneous crust versus age, *Geophys. J. Int.*, *124*, 631–635, doi:10.1111/j.1365-246X.1996.tb07041.x.

Grevemeyer, I., W. Weigel, and C. Jennrich (1998), Structure and ageing of oceanic crust at 14°S on the East Pacific Rise, *Geophys. J. Int.*, *135*, 573–584, doi:10.1046/j.1365-246X.1998.00673.x.

Grevemeyer, I., N. Kaul, H. Villinger, and W. Weigel (1999), Hydrothermal activity and the evolution of the seismic properties of upper oceanic crust, *J. Geophys. Res.*, *104*(B3), 5069–5079, doi:10.1029/1998JB900096.

Huang, P. Y., and S. C. Solomon (1987), Centroid depths and mechanisms of Mid-Ocean Ridge earthquakes in the Indian Ocean, Gulf of Aden, and Red Sea, *J. Geophys. Res.*, *92*(B2), 1361–1382, doi:10.1029/JB092iB02p01361.

Huang, P. Y., and S. C. Solomon (1988), Centroid depths of mid-ocean ridge earthquakes: Dependence on spreading rate, *J. Geophys. Res.*, *93*(B11), 13,445–13,477, doi:10.1029/JB093iB11p13445.

Ildefonse, B., D. K. Blackman, B. E. John, Y. Ohara, D. J. Miller, and C. J. MacLeod (2007), Oceanic core complexes and crustal accretion at slow-spreading ridges, *Geology*, *35*, 623–626, doi:10.1130/G23531A.1.

Karson, J. A., et al. (1987), Along-axis variations in seafloor spreading in the MARK area, *Nature*, *328*, 681–685, doi:10.1038/328681a0.

Karson, J. A., G. L. Früh-Green, D. S. Kelley, E. A. Williams, D. R. Yoerger, and M. Jakuba (2006), Detachment shear zone of the Atlantis Massif core complex, Mid-Atlantic Ridge, 30°N, *Geochem. Geophys. Geosyst.*, *7*, Q06016, doi:10.1029/2005GC001109.

Korenaga, et al. (2000), Crustal structure of the southeast Greenland margin from joint refraction and reflection seismic tomography, *J. Geophys. Res.*, *105*(B9), 21,591–21,614, doi:10.1029/2000JB900188.

Leblanc, M., G. Ceuleneer, H. Al Azri, and J. Jedwab (1991), Concentration hydrothermale de Pd et de Pt dans les péridotites mantellaires du complexe ophiolitique d'Oman, *C.R. Acad. Sci.*, *312*(II), 1007–1012.

Luetgert, J. H. (1992) Interactive two-dimensional seismic raytracing for the Macintosh, *U.S. Geological Survey, Open-File Report 92–356*, 44.

Maia, M., and P. Gente (1998), Three-dimensional gravity and bathymetry analysis of the Mid-Atlantic Ridge between 20°N and 24°N: Flow geometry and temporal evolution of the segmentation, *J. Geophys. Res.*, *103*(B1), 951–974, doi:10.1029/97JB01635.

Muller, M. R., T. A. Minshull, and R. S. White (2000), Crustal structure of the Southwest Indian Ridge at the Atlantis II fracture zone, *J. Geophys. Res.*, *105*(B11), 25,809–25,828, doi:10.1029/2000JB900262.

Natland, J. H., and H. J. B. Dick (1996), Melt migration through high-level gabbroic cumulates of the East Pacific rise at Hess deep: The origin of magma lenses and the deep crustal structure of fast spreading ridges, in Proc. Ocean Drilling Program, Scientific Results vol. 147, edited by C. Mevel, K. M. Gillis, J. F. Allan, and D. Elthon, pp. 21–59, College Station, Ocean Drilling Program, Texas, doi:10.2973/odp.proc.sr.147.002.1996.

Nedimović, M. R., S. M. Carbotte, J. B. Diebold, A. J. Harding, J. P. Canales, and G. M. Kent (2008), Upper crustal evolution across the Juan de Fuca ridge flanks, *Geochem. Geophys. Geosyst.*, *9*, Q09006, doi:10.1029/2008GC002085.

Nur, A., H. Ron, and O. Scotti (1986), Fault mechanics and the kinematics of block rotations, *Geology*, *14*, 746–749, doi:10.1130/0091-7613(1986)14<746:FMATKO>2.0.CO;2.

Planert, L., E. R. Flueh, F. Tilmann, I. Grevemeyer, and T. J. Reston (2010), Crustal structure of a rifted oceanic core complex and its conjugate side at the MAR at 5°S: Implications for melt extraction during detachment faulting and core complex formation, *Geophys. J. Int.*, *181*, 113–126.

Purdy, G. M., and R. S. Detrick (1986), Crustal structure of the Mid-Atlantic Ridge at 23°N from seismic refraction studies, *J. Geophys. Res.*, *91*(B3), 3739–3762, doi:10.1029/JB091iB03p03739.

Python, M., G. Ceuleneer, Y. Ishida, J. A. Barrat, and S. Arai (2007), Oman diopsidites a new lithology diagnostic of very high temperature hydrothermal circulation in mantle peridotite below oceanic spreading centres, *Earth Planet. Sci. Lett.*, *255*, 289–305, doi:10.1016/j.epsl.2006.12.030.

Ranero, C. R., and T. J. Reston (1999), Detachment faulting at ocean core complexes, *Geology*, *27*, 983–986, doi:10.1130/0091-7613(1999)027<0983:DFAOCC>2.3.CO;2.

Reston, T. J., W. Weinrebe, I. Grevemeyer, E. R. Flueh, N. C. Mitchell, L. Kirstein, C. Kopp, H. Kopp, et al. (2002), A rifted inside corner massif on the Mid-Atlantic Ridge at 5°S, *Earth Planet. Sci. Lett.*, *200*, 155–169, doi:10.1016/S0012-821X(02)00636-2.

Reston, T. J., C. R. Ranero, O. Ruoff, M. Peres-Gussinye, and J. J. Dañobeitia (2004), Geometry of extensional faults developed at slow-spreading centres from pre-stacked depth migration of seismic reflection data in the Central Atlantic (Canary Basin), *Geophys. J. Int.*, *159*, 591–606, doi:10.1111/j.1365-246X.2004.02444.x.

Ross, K., and D. Elthon (1997), Cumulus and postcumulus crystallization in the oceanic crust: Major and trace-element geochemistry of Leg 153 gabbroic rocks, in Proc. Ocean Drilling Program, Scientific Results, vol. 153, edited by J. A. Karson, M. Cannat, D. J. Miller, and D. Elthon, pp. 23–34, College Station, Ocean Drilling Program, Texas, doi:10.2973/odp.proc.sr.153.023.1997.

Smith, D. K., J. Escartin, M. Cannat, M. Tolstoy, C. G. Fox, D. R. Bohnenstiel, and S. Basin (2003), Spatial and temporal distribution of seismicity along the Mid-Atlantic Ridge (15°–35°N), *J. Geophys. Res.*, *108*(B3), 2167, doi:10.1029/2002JB001964.

Smith, D. K., J. Escartın, H. Schouten, and J. R. Cann (2008), Fault rotation and core complex formation: Significant processes in seafloor formation at slow-spreading mid-ocean ridges (Mid-Atlantic Ridge, 13°–15°N), *Geochem. Geophys. Geosyst.*, *9*, Q03003, doi:10.1029/2007GC001699.

Smith, D. K., J. R. Cann, and J. Escartin (2006), Widespread active detachment faulting and core complex formation near 13°N on the Mid-Atlantic Ridge, *Nature*, *442*, 440–443, doi:10.1038/nature04950.

Stevenson, J. M., J. A. Hildebrand, and M. A. Zumberge (1994), An ocean bottom gravity study of the southern Juan de Fuca Ridge, *J. Geophys. Res.*, *99*(B3), 4875–4888, doi:10.1029/93JB02076.

Tilmann, F., E. Flueh, L. Planert, T. Reston, and W. Weinrebe (2004), Microearthquake seismicity of the Mid-Atlantic Ridge at 5°S: A view of tectonic extension, *J. Geophys. Res.*, *109*(B6), B06102, doi:10.1029/2003JB002827.

Toomey, D. R., S. C. Solomin, and G. M. Purdy (1988), Microearthquakes beneath the median valley of the Mid-Atlantic Ridge near 23°N: Tomography and tectonics, *J. Geophys. Res.*, *93*(B8), 9093–9112, doi:10.1029/JB093iB08p09093.

Tucholke, B. E., and J. Lin (1994), A geological model for the structure of ridge segments in slow spreading ocean crust, *J. Geophys. Res.*, *99*(B6), 11,937–11,958, doi:10.1029/94JB00338.

Tucholke, B. E., J. Lin, and M. C. Kleinrock (1998), Megamullions and mullion structure defining oceanic metamorphic core complexes on the Mid-Atlantic Ridge, *J. Geophys. Res.*, *103*(B5), 9857–9866, doi:10.1029/98JB00167.

White, R. S., D. McKenzie, and R. K. O'Nions, (1992), Oceanic crustal thickness from seismic measurements and rare earth element inversions, *J. Geophys. Res.*, *97*(B13), 19 683–19 715.

A. Dannowski and I. Grevemeyer, Leibniz Institut für Meereswissenschaften, IFM-GEOMAR, Wischhofstr. 1-3, 24 148 Kiel, Germany. (adannowski@ifm-geomar.de)

C. R. Ranero, ICREA at Institut de Ciencias del Mar, CSIC, Pg. Marítim de la Barceloneta 37-49, 08003 Barcelona, Spain.

G. Ceuleneer, Toulouse University, Observatoire Midi-Pyrénées, CNRS-UMR5562, 14 Avenue E. Belin, 31400 Toulouse, France.

M. Maia and P. Gente, Université Européenne de Bretagne, CNRS UMR 6538, Brest, France.

J. P. Morgan, EAS Department, Cornell University, Ithaca, NY 14853, USA.